MODELING OF CNTs/NANOCOMPOSITES DEFORMATIONS AND TENSILE FRACTURE

Aleksander Muc
Cracow University of Technology, Institute of Machine Design
Kraków, Poland
olekmuc@mech.pk.edu.pl

SUMMARY

A 3D nonlinear finite element model for single-walled carbon nanotubes with atom vacancy defects is proposed. The model is consistent with molecular mechanics formulations. Assuming defects in CNTs their influence on nanocomposite properties is discussed. The results are presented in the form of the strain-stress relations. The effective properties are evaluated with the use of the homogenization theory.

Keywords: Carbon Nanotubes, Nanocomposites, Vacancy Defects, Numerical Analysis.

INTRODUCTION

Carbon nanotubes (CNTs) hold considerable promise as ultra-stiff high-strength fibers for use in cabling and nanocomposites. The outstanding mechanical characteristics hold for nearly perfect CNTs. Several theoretical studies have reported CNT failure strains in the range of 20–30% and failure stresses usually in excess of 100 GPa. By contrast, the few direct mechanical measurements that have been reported indicate much lower values. Most attempts to resolve the theoretical–experimental discrepancies have concentrated on the possible role of defects in limiting peak strengths. If CNTs have defects in the atomic network, one can expect that due to their quasi-one-dimensional atomic structure even a small number of defects will result in some degradation of their characteristics. The defects can appear at the stage of CNT growth and purification, or later on during device or composite production. Moreover, defects in CNTs can deliberately be created by chemical treatment or by irradiation to achieve the desired functionality. Therefore, possible defects in CNTs can be classified in the following manner:

- Point defects such as vacancies,
- Topological defects caused by forming pentagons and heptagons e.g. 5-7-7-5 defect – so-called Stone-Wales defects,
- Hybridization defects caused due to functionalisation.

Different approaches have been used to explore the role of vacancy defects in the fracture of CNTs under axial tension. In general, they can be divided into two groups: single- or two-atom vacancy defects Mielke et al. [1-5] or axisymmetric fracture patterns (defects) [6, 7]. However, the majority of existing works deals with the analysis of the Stone-Wales transformation that results in ductile fracture for nanotubes [8-11].

Significant challenges exist in both the micromechanical characterization of nanotubes and their composites and the modeling of the elastic and fracture behavior at the nano-scale. In general they include (a) complete lack of micromechanical characterization techniques for direct property measurement, (b) tremendous limitations on specimen size, (c) uncertainty in data obtained from indirect measurements, and (d) inadequacy in test specimen preparation techniques and lack of control in nanotube alignment and distribution. The above-mentioned problems and the description of nanocomposites fracture modeling are discussed in Refs [12-15].
It is worth to point out that the theoretical analysis of CNTs and nanocomposites fracture problems has adopted: the atomistic approaches (classical molecular dynamics (MD) and mechanics (MM)) and the continuum mechanics approaches.

INTERATOMIC POTENTIALS

To capture the essential feature of chemical bonding in graphite Brenner [16] established an interatomic potential (called as the REBO potential) for carbon in the following form:

$$V=V_R(r_{ij})-B_{ij}V_A(r_{ij}),\ V_R(r)=\frac{D_{(e)}}{S-1}exp\left[-\sqrt{2S}\beta(r-R)\right],\ V_A(r)=\frac{D_{(e)}S}{S-1}exp\left[-\sqrt{2/S}\beta(r-R)\right] \quad (1)$$

where r_{ij} is the distance between atoms i and j, and the parameter B_{ij} is given by:

$$B_{ij}=\left[1+\sum_{k(\neq i,j)}G(\theta_{ijk})\right]^{-\delta},\ G(\theta)=a_0\left[1+\frac{c_0^2}{d_0^2}+\frac{c_0^2}{d_0^2+(1+cos\theta)^2}\right],\qquad \overline{B}_{ij}=(B_{ij}+B_{ji})/2 \quad (2)$$

where θ_{ijk} is the angle between bonds i _ j and i _ k, and the set of material parameters is adopted here as follows:

D_e = 0.9612 nN nm; S=1.22; β=21 nm^{-1}; R= 0.139 nm; δ= 0.5, a_0 = 0.00020813,

c_0=330, d_0=3.5 (3)

For nanocomposites the bonding between the nanotube and the matrix is in general modeled by van der Waals interactions. For simulations of van der Waals interactions the Lennard-Jones ‘‘6–12’’ potential is adopted herein and is written as:

$$V(r_{ij})=4\varepsilon\left[\left(\frac{\sigma}{r_{ij}}\right)^{12}-\left(\frac{\sigma}{r_{ij}}\right)^{6}\right] \quad (4)$$

For carbon atoms the Lennard-Jones parameters are ε = 0.0556 kcal/mole and σ = 3.4A˚ [15].

NUMERICAL MODEL

Carbon Nanotubes

In the present study a numerical efficient formulation for modeling CNTs is presented based on the geometrically exact theory together with a fnite element discretization incorporating atomistic potentials. This approach offers several advantages primarily related to the model's computational efficiency and to the possibility of a simple implementation into existing commercial FE codes.

Let us consider that the hexagon, which is the constitutional element of CNTs nano-structure, is simulated as structural element of a space-frame made of 3D beams . Of course, in the same way the entire nanotube lattice may be modelled. The simulation leads to the correspondence of the bond length C–C with the 3D beam element length L and with the element diameter d characterizing a circular cross-sectional area for the element. The linkage between molecular and continuum mechanics can be made by an appropriate definition of 3D beam mechanical properties.

Based on the energy equivalence between local potential energies in computational chemistry and elemental strain energies in structural mechanics, we can determine the tensile resistance, the flexural rigidity and the torsional stiffness for an equivalent beam. If the beam element is assumed to be of round section, then only three stiffness parameters, i.e., the tensile resistance EA, the flexural rigidity EI and the torsional stiffness GJ, need to be determined for deformation analysis. By considering the energy equivalence, a direct relationship between the structural mechanics parameters and the molecular mechanics force field constants can be established [15], i.e.:

$$\frac{E_i A_i}{r_i}=k_{ri},\ \frac{E_i I_i}{r_i}=k_{\theta i},\ \frac{G_i J_i}{r_i}=k_{ti} \tag{5}$$

where k_{ri}, $k_{\theta i}$ and k_{ti} are the force field constants in molecular mechanics. They are indexed by the number of the beam occurring in the RVE for a given nanotube structure. For zigzag and armchair configurations the RVE are plotted in Fig.1.

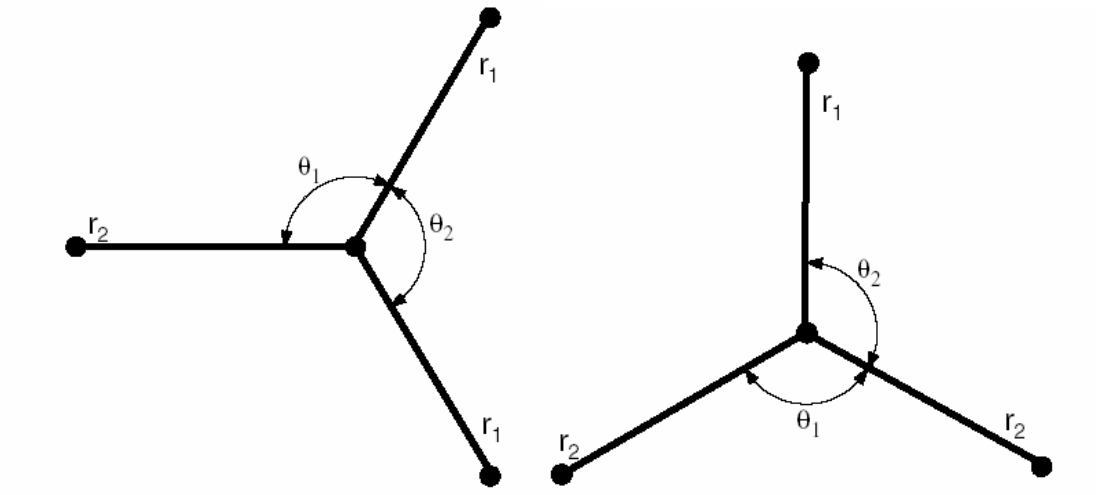

Fig. 1 Representative volume elements of an a) armchair CNT and b) zigzag CNT.

Let us note that the present formulation is an extension of the models proposed in Refs [7,15], and on the other hand, it incorporates special features of molecular mechanics models. In addition, it allows to analyze large deformations of CNTs since the beam length L in Eqn (5) is replaced by an actual beam length r_i different for different beams in the RVE.
By comparing energies of the mechanical and molecular diatomic systems the force constants k_{ri}, $k_{\theta i}$ can be derived. Using the interatomic potentials shown in Eqs (1) and (4), the stretching force that results from the bond elongation Δr_i and the twisting moment that results from the bond angle variation $\Delta\theta_i$ can be calculated as follows:

$$F(\Delta r_i)=\frac{\partial V}{\partial r_i},\ M(\Delta\theta_i)=\frac{\partial V}{\partial\theta_i},\ \Delta r_i=r_i-r_{0i},\ \Delta\theta_i=\theta_i-\theta_{0i},\ i=1,2 \tag{6}$$

The derivatives in Eqn (6) are expanded in the Taylor series up to the first derivative (linear terms) only. However the initial values r_{0i} and θ_{0i} are modified at each iteration step since, in fact, both the stretching forces and the twisting moments are nonlinear with respect to the bond length and to the bond angle, respectively.
By assuming a circular beam section with diameter d_i, and setting $A_i=\pi d^2/4$, $I_i=\pi d^4/64$, Eqs. (5,6) give:

$$d_i=4\sqrt{\frac{k_{\theta i}}{k_{ri}}},\ E_i=\frac{k_{ri}^2 r_i}{4\pi k_{\theta i}} \tag{7}$$

Then, following the procedure of the finite element structural mechanics technique, the nanotube deformation under certain loading conditions can be readily solved. It is worth to note that Young's moduli E_1 and E_2 are different even for the linear part of the stress-strain curve since the beam lengths r_i are different at each iteration step, and the force constants k_{ri} and $k_{\theta i}$ are nonlinear functions of r and θ, respectively, as the second derivatives of the interatomic potential.

Nanocomposites

The nanotube is modeled at the atomistic scale (see the previous section) whereas the polymeric matrix is much more convenient to treat as a continuum. For convenience, the CNTs are considered as straight fibers embedded in the composite. Therefore, for simulations of van der Waals interactions at the nanotube/polymer interface, a truss rod model is adopted – see Li, Chou [15]. It is assumed that the nanotube is embedded in the matrix (Fig. 2a). Because the volume of the matrix is usually much greater than that of the reinforcement, the polymeric matrix is modeled as a continuum with the use of the classical 3D finite elements. At the nanotube/polymer interface 3D finite elements are connected with the CNTs by a system of rods (Fig, 2a). It is assumed that the rods at the nanotube/polymer interface have the length less than 0.4 [nm]. The Lennard-Jones potential describes the mechanical properties of the rods.

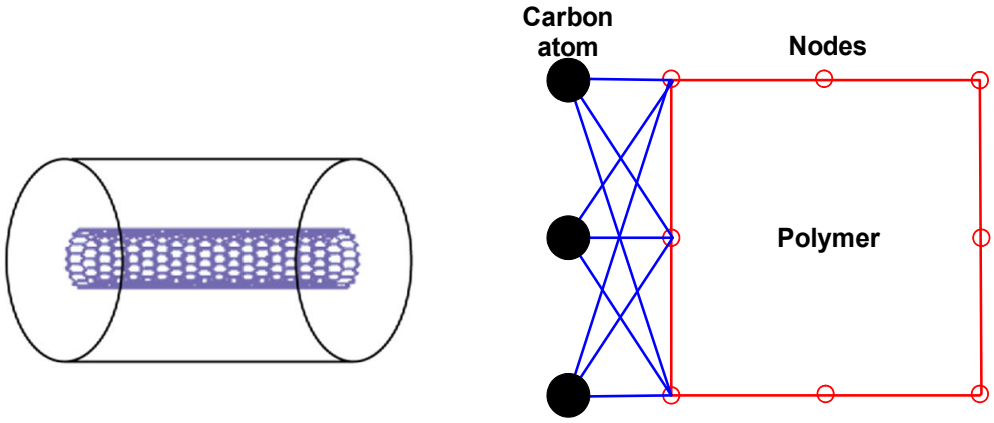

a) b)

Fig.2 Nanotube/polymer interface

Modeling of atom vacancies

Let us assume that a single atom is removed from the lattice being a pristine tube. Thus, 12-membered ring (two hexagons) can be reconstructed for instance to a five-membered ring and a nine-membered ring – see Fig.3, and finally we obtain non-axisymmetric CNTs.

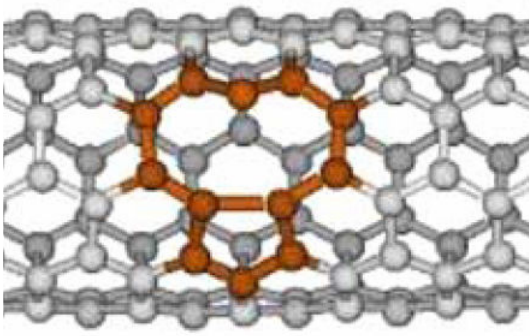

Fig.3 The one-atom vacancy defect

Of course, using the similar approach it is possible to model various types of defects.

NUMERICAL RESULTS

In our approach the Young's modulus of a material is defined as the ratio of longitudinal stress to longitudinal strain as obtained from a uni-axial tension test. Following this definition, the Young's modulus of CNTs is been calculated using the following equation:

$$E_{long}=\frac{\langle\sigma_{long}\rangle}{\langle\varepsilon_{long}\rangle},\ \langle\sigma_{long}\rangle=\sum_{k=1}^{N_{beams}}\sigma^{k}_{long},\ \langle\varepsilon_{long}\rangle=\sum_{k=1}^{N_{beams}}\varepsilon^{k}_{long} \tag{17}$$

where $\langle\sigma_{long}\rangle/\langle\varepsilon_{long}\rangle$ is an average longitudinal stress/strain component computed as the sum of longitudinal components of each individual beams characterizing C-C bonds. Let us note that the above definition is more general than that described as the global on in the first section and it is consistent with the homogenization theory. For nanocomposites the average values are supplemented by the components obtained from the FE characterizing polymeric matrix and the nanotube/polymer interface (see Fig.2). At each load step corresponding to the increments of the axial displacements, the molecular mechanics force field constants with the use of Eqn (6) as well as the beam geometrical and mechanical properties – Eqn (7) are evaluated in order to find the longitudinal stress components in individual beams. This iterative, non-linear procedure goes on to the prescribed end of the deformation process. The accuracy of modeling procedure depends on the number of load steps chosen. In order to maximize the accuracy of computational results, in each case, the displacement increment was chosen from convergence tests in which the convergence criterion was set equal to 2% of the maximal stress. Thereby, if between two sequential displacement increments a difference smaller than the 2% was achieved in the computed maximal stress, the larger displacement increment was finally adopted for the analysis.

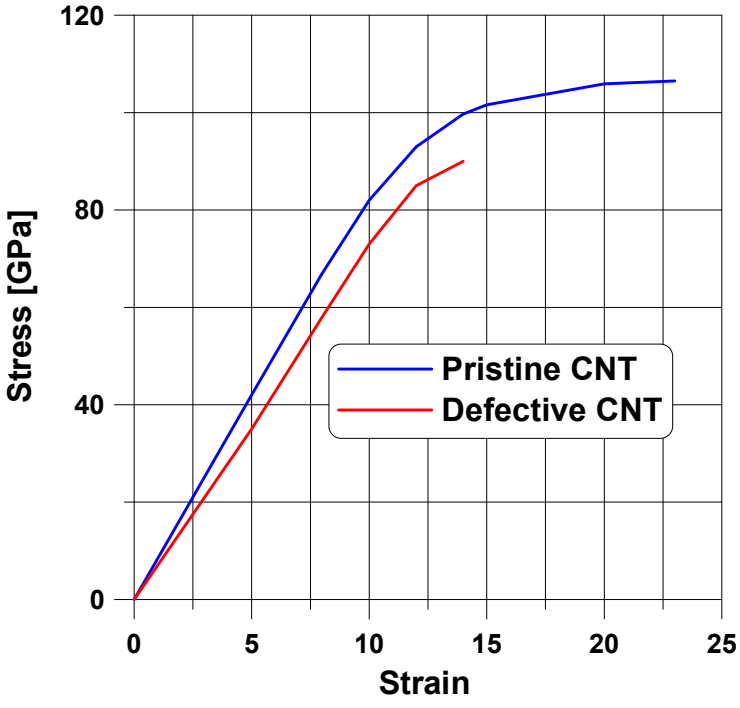

Fig. 4 Tensile stress-strain curves for pristine and defective (5,5) nanotube

Figure 4 shows the calculated stress-strain curves and Young's modulus of pristine and defective (with one-atom vacancy) carbon nanotubes from the present models. At the

beginning we have compared the Young's moduli of (5,5) armchair CNTs. The predicted initial Young's modulus of CNTs are 797 GPa and 708 GPa for the pristine and defective CNT, respectively, which agrees well with the experimental value and other theoretical values mentioned previously. Those values are strongly dependent on the form of the assumed interatomic potential and the form of defects. The defects reduce the failure stresses by 19 %, and failure strains by 32 %. It may reduce also buckling stresses for compressive loads since the defect considered may be treated as an geometrical imperfection for cylindrical shells. It is also obvious that the reduction factor is significantly dependent on the form and magnitude of imperfections (the assumed type of defects).
For CNT with defect considerable bond angle change are observed. Some of the initial bond angles deviate considerably from perfect tube.

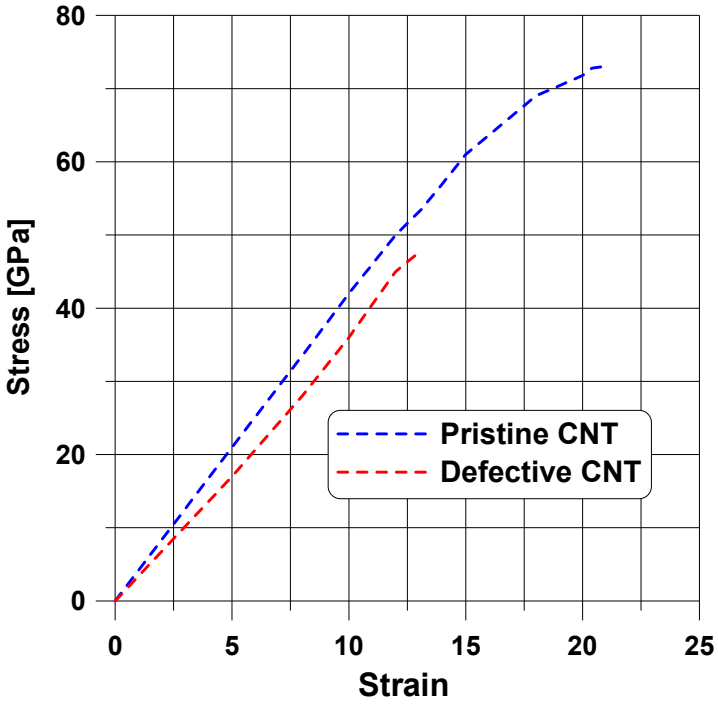

Fig 5. Tensile stress-strain curves for pristine and defective nanocomposites reinforced by the armchair (5,5) nanotube (4% wt)

Here, we calculate the critical strains of defect nucleation and fracture of CNTs embedded in a matrix by using our numerical/mechanics model. The interaction of CNTs in a composite may influence their deformation and fracture behaviors. the Young's modulus and Poisson's ratio of the matrix are taken as E_m =40GPa and ν_m =0.2, respectively.
Figure 5 illustrates the stress-strain curves for nanocomposites reinforced by perfect and imperfect CNTs – the imperfection has the form presented in Fig. 3.
It is found that when a CNT is placed in a composite, its critical strain of breaking will decrease. The critical strain of fracture of the (5,5) CNT is about 22.4 %, and reduces to 21.3% after it is embedded in the composite. Similarly, the critical strain of breaking of the defective (5,5) CNT decreases from 14.3% to 13.1% after it is put into the composite. This might also be attributed to the constraint effect of the matrix. A CNT

embedded in a composite is less effective to release the energy, and becomes easier to fracture than that not embedded. In the present paper, we do not consider the fracture of the polymer matrix though in reality most polymers cannot sustain such a high tensile strain. The above effects are also associated with the reduction of Young's modulus and the critical (failure) stresses. The values of critical strains and stresses are highly affected by the assumed values of the matrix Young's modulus. The critical strains decrease with the increase of the value E_m.

ACKNOWLEDGEMENTS

The Polish Research Foundation PB 1174/B/T02/2009/36 is gratefully acknowledged for financial support.

References

1. Troya, D., Mielke, S.L., Schatz, G.C., Carbon nanotube fracture – differences between quantum mechanical mechanisms and those of empirical potentials, Chemical Physics Letters 382 (2003) 133–141
2. Mielke, S.L. et al., The role of vacancy defects and holes in the fracture of carbon nanotubes, Chemical Physics Letters 390 (2004) 413–420.
3. Liew, K.M., He, X.Q., Wong, C.H., On the study of elastic and plastic properties of multi-walled carbon nanotubes under axial tension using molecular dynamics simulation, Acta Materialia 52 (2004) 2521–2527
4. Mielke, S.L. et al., The effects of extensive pitting on the mechanical properties of carbon nanotubes, Chemical Physics Letters 446 (2007) 128–132
5. Zhang, S. et al., Mechanics of defects in carbon nanotubes: Atomistic and multiscale simulations**,** Pysical Review **71**, 115403 s2005d
6. Duan, W. H. et al., Molecular mechanics modeling of carbon nanotube fracture, Carbon 45 (2007) 1769–1776
7. Tserpes, K.I., Papanikos, P., Tsirkas, S.A., A progressive fracture model for carbon nanotubes, Composites: Part B 37 (2006) 662–669
8. Nardelli, M.B., Yakobson, B. I., Bernholc, J., Brittle and ductile behavior in carbon nanotubes. Physical Review Letters 1998; 81(21):4656–9.
9. Lu, J., Zhang, L., Analysis of localized failure of single-wall carbon nanotubes, Computational Materials Science 35 (2006) 432–441
10. Song, J. et al., Stone–Wales transformation: Precursor of fracture in carbon nanotubes, International Journal of Mechanical Sciences 48 (2006) 1464–1470
11. Zhang, P. et al., An atomistic-based continuum theory for carbon nanotubes: analysis of fracture nucleation, Journal of the Mechanics and Physics of Solids 52 (2004) 977 – 998
12. Wagner HD, Lourie O, Feldman Y, Tenne R. Stress-induced fragmentation of multiwall carbon nanotubes in a polymer matrix. Applied Physics Letters 1998;72(2):188–90.

13. Lourie O, Wagner HD. Transmission electron microscopy observations of fracture of single-wall carbon nanotubes under axial tension. Applied Physics Letters 1998;73(24):3527–9.
14. Shi, D.-L. et al., Multiscale analysis of fracture of carbon nanotubes embedded in composites, International Journal of Fracture (2005) 134:369–386
15. Li, C., Chou, T.-W., Multiscale modeling of compressive behavior of carbon nanotube/polymer composites, Composites Science and Technology 66 (2006) 2409–2414
16. Brenner DW. Empirical potential for hydrocarbons for use in simulating the chemical vapor deposition of diamond films. Physical Review B 1990;42:9458–71.

Previous Paper ***Back to Programme*** ***Back to Topic***